Journal of Materials Research and Technology 27 (2023) 7110–7118

Contents lists available at ScienceDirect

Journal of Materials Research and Technology

journal homepage: www.elsevier.com/locate/jmrt

Improving the machinability of the high-entropy alloy CoCrFeMnNi by in-situ laser-assisted diamond turning

Hanheng Du [a,1], Yidan Wang [b,1], Yuhan Li [a], Sen Yin [a], Denghui Li [a], Wai Sze Yip [a,c,*], Suet To [a,c,**]

[a] State Key Laboratory of Ultra-precision Machining Technology, Department of Industrial and Systems Engineering, The Hong Kong Polytechnic University, Hong Kong, China
[b] State Key Laboratory of High-performance Precision Manufacturing, Dalian University of Technology, China
[c] The Hong Kong Polytechnic University Shenzhen Research Institute, Shenzhen, China

ARTICLE INFO

Keywords:
Ultra-precision diamond turning
Laser-assisted machining
High-entropy alloy
Mirror surface
CoCrFeMnNi

ABSTRACT

High-entropy alloys, as the novel multi-principal alloys composed of five or more elements in equal-atomic ratios or near-equal atomic ratios, are widespread in extreme environments, including high-temperature, high-dynamic loading, and high-irradiation. However, how to improve their machinability still faces challenges because of their high hardness and wear resistance. To solve this problem, this paper proposes an in-situ laser-assisted diamond turning process. Experimental results show the machinability of the high-entropy alloy CoCrFeMnNi is obviously improved. The average value of the surface roughness Sa of the machined sample reaches 2 nm. Compared with the traditional single-point diamond turning, the surface quality is improved by 33.3 %, demonstrating the effectiveness of the proposed machining method. Tool wear also decreases by above 35 %, again demonstrating the superiority of the proposed machining method. Besides, the effect of the machining on the crystalline structure is also analyzed. Therefore, this study provides an efficient and simple approach for enhancing the machinability of the high-entropy alloy CoCrFeMnNi, which can be applied in industrial production in the future.

1. Introduction

High-entropy alloys are complex alloys that have significantly increased the number of alloy systems available, resulting in alloys with guaranteed structural and functional properties [1–3]. High-entropy alloys are also a relatively new class of metallic materials with exceptional thermophysical properties [4,5]. They differ from traditional alloys with one or two main elements, which are common in many engineering alloys. High-entropy alloys use at least five principal elements in proportions of 5 %–35 % and exhibit solid structure features [6–12]. These alloys can have an exceptional combination of material properties, such as superior ductility, high strength, fracture toughness, superior mechanical properties at extremely high temperatures, and excellent corrosion, oxidation, and creep resistance [13–16]. Because of their exceptional properties, these alloys hold the promise of being utilized as structural components in a wide range of engineering applications [17].

According to the literature, high-entropy alloys including CoCrFeMnNi are produced using both liquid-state and solid-state processing techniques [18]. Vacuum arc melting has been identified as one of the most common methods of liquid-state processing for high-entropy alloys. To prevent oxidation during the liquid state processing, metallic alloy ingots or particulate elements are subjected to heat treatment in an electric furnace or using a tungsten electric arc in an argon environment [19]. However, limitations with liquid state processing have been discovered: evaporation of substances with low melting temperatures; and the formation of heterogeneous compounds due to a low solidification rate [20]. The method for developing solid-state processing of

* Corresponding author. State Key Laboratory of Ultra-precision Machining Technology, Department of Industrial and Systems Engineering, The Hong Kong Polytechnic University, Hong Kong, China.
** Corresponding author. State Key Laboratory of Ultra-precision Machining Technology, Department of Industrial and Systems Engineering, The Hong Kong Polytechnic University, Hong Kong, China.
E-mail addresses: lenny.ws.yip@polyu.edu.hk (W.S. Yip), sandy.to@polyu.edu.hk (S. To).
[1] These authors contributed equally to this work.

https://doi.org/10.1016/j.jmrt.2023.11.119
Received 11 August 2023; Received in revised form 5 November 2023; Accepted 14 November 2023
Available online 17 November 2023

high-entropy alloys is also extensively implemented and explicitly mentioned. In solid-state processing, fine metallic materials are blended at room temperature and subsequently consolidated at elevated temperatures. Aside from liquid-state and solid-state processing techniques, there has been a significant increase in the number of research studies involving mechanically alloyed high-entropy alloys over the last decade. The various high-entropy alloys are created using various methods while retaining their essential properties and significance. Several studies have demonstrated the printability of high-entropy alloys using electron beam melting [21–23]. The findings suggest that additive manufacturing could produce nearly completely dense samples with superior tensile properties. Despite this, the surface quality and geometric accuracy of high-entropy alloys CoCrFeMnNi manufactured by additive manufacturing cannot still meet the standards required for industrial use due to the characteristics of the powder-based layer-by-layer deposition process [12]. Processing high-entropy alloys with welding technologies such as friction stir welding and electron beam welding [24] have, on the other hand, been the subject of numerous studies to date, however, the surface quality does not fulfill the precision level in practical uses. As a result, additional machining procedures are required to enhance the surface quality of high-entropy alloys CoCrFeMnNi. On the other hand, CoCrFeMnNi is difficult to machine due to its unique composition and material properties. The high-entropy alloy is made up of five distinct elements in atomic proportions that are relatively similar, resulting in a material with a complex microstructure and a high level of atomic disorder [25]. This atomic disorder makes it difficult for dislocations to migrate within the material, resulting in unfavorable machining hardness and difficulty in machining. The presence of multiple elements disrupts the crystal lattice and reduces machinability, resulting in decreased tool life. Currently, only a few researchers have utilized milling to investigate its machinability [26]. However, the surface roughness achieved through milling is at the micrometer level (Ra = ~1 μm), which does not meet the precision compound requirements. The single-point diamond turning is a well-established machining method capable of achieving nanometer-level surface quality.

In-situ laser-assisted machining has been demonstrated to further enhance the surface quality of the difficult-to-machine material [27–30]. In-situ laser-assisted machining combines laser heating and material removal in a single manufacturing step [30–33]. During in-situ laser-assisted machining, a laser beam is directed onto the workpiece cutting zone while the material is removed by the cutting tool. The laser heats the material, changing its hardness and ductility to make it more machinable [29,33–35]. Furthermore, laser heating can cause desirable microstructural changes in the alloy that improve its mechanical properties [31], such as the formation of fine and equiaxed grains, which improves its strength and makes it suitable for machining. In-situ laser-assisted machining has the potential to improve the machinability of the high-entropy alloy by modifying the machined surface properties and the microstructure, resulting in better surface finish and machining efficiency while also producing a desirable microstructure that improves its mechanical properties. Because of the imbalanced mechanical performance of the high-entropy alloy, in-situ laser-assisted machining can be especially beneficial. During machining, laser heating can make it less prone to deformation and fracture [27,36–39].

As one of the promising machining technologies for fabricating micro-scale components, ultra-precision machining on high-entropy alloys should have excellent capability. However, no extensive research on ultra-precision machining of CoCrFeMnNi has been conducted to date. As a result, we must investigate this matter so that their applications can be processed. This paper proposes an in-situ laser-assisted diamond turning (LADT) approach to address the challenges of machining CoCrFeMnNi with nano-scale. In this approach, the in-situ laser-assisted machining is combined with the single-point diamond turning. According to the results of experiments in this study, the machinability of the high-entropy alloy CoCrFeMnNi appears to be improved by in-situ laser-assisted diamond turning process. Surface quality is improved, and tool wear is significantly reduced when compared to traditional single-point diamond turning, demonstrating the practicality of the proposed machining approach. This paper also investigates the effect of machining on the crystalline structure. This research suggests a practical method for improving the machinability in the nano-scale of the high-entropy alloy CoCrFeMnNi, which could be used in manufacturing processes, as the demand for micro-components significantly increases.

2. Methods

2.1. Sample preparation

The equiatomic ratio CoCrFeMnNi sample was made by the vacuum induction melting of high-purity (more than 99.8 %) raw materials. All alloying elements were cleaned using acetone before putting the raw materials into the crucible. Then, the chamber of the vacuum induction melting furnace was vacuumed and then filled with argon. The melting temperature was kept at about 1500 °C. In order to ensure chemical composition homogeneity, this alloy was re-melted three times. After cooling in the furnace, the ingot was cut by low-speed wire electrical to the dimension of 10 mm × 10 mm × 5 mm for the next in-situ laser-assisted diamond turning experiments. The initial surface roughness (Sa) of the sample is around 2.5 μm. The energy-dispersive X-ray spectroscopy (EDS) mapping of the sample surface is shown in Fig. 1, which shows the five elements are equally distributed in the sample. This guarantees the uniformity and quality of samples, which helps the next comparison study of different machining processes.

2.2. In-situ laser-assisted diamond turning process

Compared with copper alloy or aluminum alloy, the high-entropy alloy CoCrFeMnNi has higher hardness and strength. When the material hardness increases greatly, the wear of the single-crystal diamond cutting tool increases when machining the workpiece [30,40,41]. As a consequence, this leads to an escalation in machining costs and a reduction in machining quality. Therefore, this study proposes an in-situ laser-assisted diamond turning (LADT) process to decrease tool wear and improve surface quality. Fig. 2 shows the schematic diagram of this process. In this process, the laser beam is emitted from the laser-assisted machining device and traverses through the single-crystal diamond of the cutting tool, finally reaching the surface of the workpiece. After absorbing the laser heat, the workpiece surface softens, and its hardness decreases. The spot size of the laser beam can be adjusted by the laser-assisted machining device. During machining, the CoCrFeMnNi sample is mounted by a fixture on the spindle of the ultraprecision lathe.

Fig. 3 shows the experimental setup of the in-situ LADT process. During machining, the CoCrFeMnNi sample with the dimension of 10 mm × 10 mm × 5 mm was fixed on the spindle of a three-axis ultraprecision lathe (450UPL, Moore Tool Co., USA) via a fixture. This ultraprecision lathe has three motion axes, namely the spindle, X-axis, and Z-axis, and all of them have extremely high motion accuracy. A single-crystal diamond cutting tool was fixed on the laser-assisted machining device (Optimus T_2, Micro-LAM, Inc., USA) that was mounted on the Z-axis via the screw. A laser power sensor was applied to measure the laser power. The laser power was set at 1.75 W in this study. And the wavelength of the laser was 1064 nm. The cutting experiments were divided into two steps: roughing machining and finishing machining. The corresponding machining parameters are determined using the orthogonal experimental method. The cutting tool specification and detailed machining parameters are listed in Table 1.

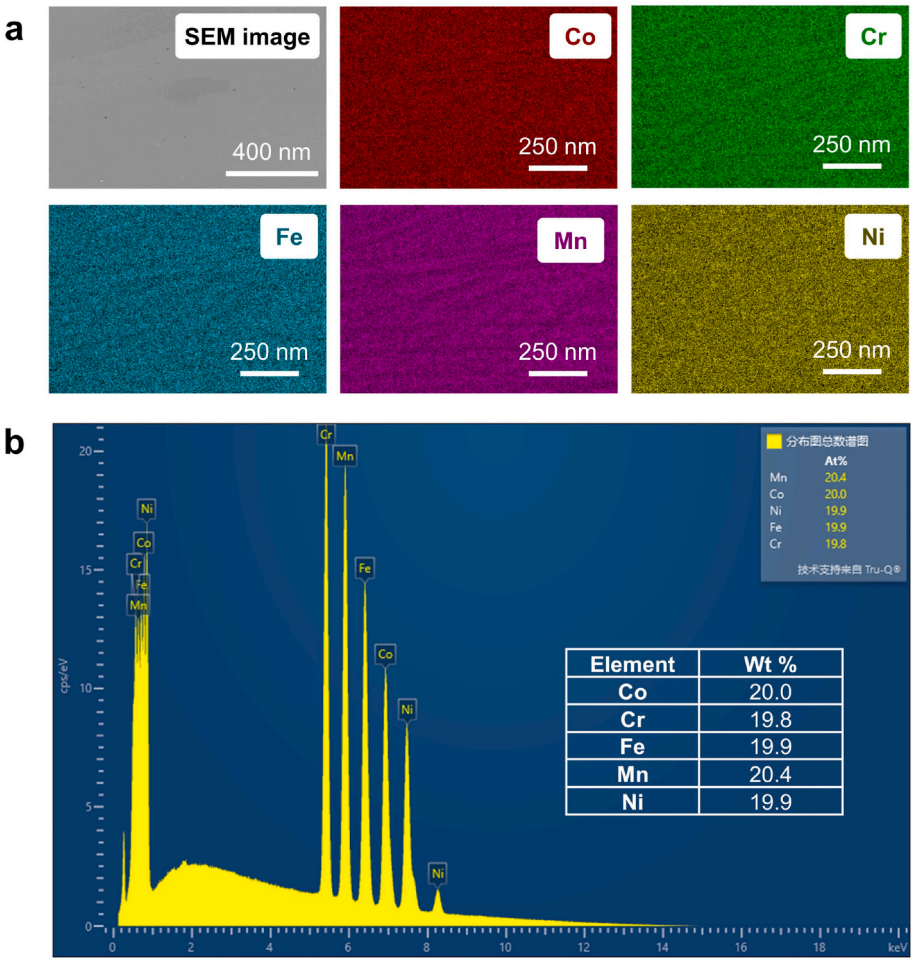

Fig. 1. EDS mapping of CoCrFeMnNi samples.

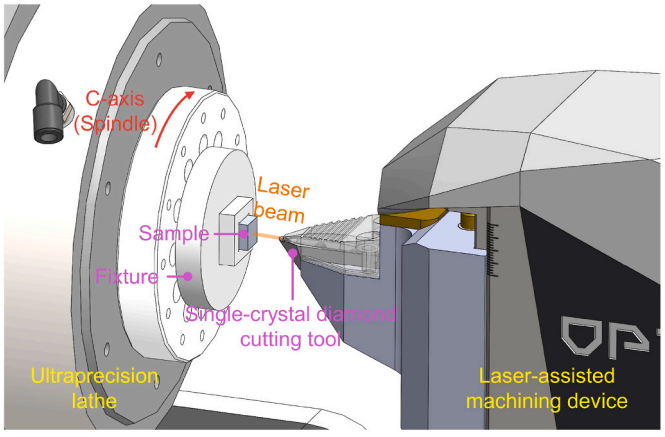

Fig. 2. Schematics of the in-situ LADT process.

3. Results and discussion

3.1. Machined surface quality

To demonstrate the effectiveness and superiority of the proposed in-situ LADT process, a comparison study was made with the traditional single-point diamond turning (SPDT) process using the same machining parameters. After machining, two samples were cleaned for 5 min using an ultrasound cleaning machine. Fig. 4 shows their photographs, which are obtained by a digital camera. And it can be found that they both have mirror surfaces.

To quantitatively characterize their machining quality, a white light interferometer (NexviewTM, Zygo Corp., USA) was applied to obtain their surface topologies and surface roughness values at two different measurement regions, as illustrated in Fig. 5. It can be found that the average value of the surface roughness of the sample after the traditional SPDT process is 3 nm, while the average surface roughness of the in-situ LADT process is 2 nm. It is decreased by 33.3 %, which obviously verifies the superiority of the proposed in-situ LADT process in this study. The cross-sectional profiles of the 213.78 μm × 213.78 μm region were also extracted to further analyze the surface quality of the two samples. In comparison with the traditional SPDT process, the proposed in-situ LADT process results in a much smoother cross-section of the sample surface. Furthermore, the arithmetic mean height (Ra) of the cross-sectional profile is 1.9 nm, which is decreased by 34.5 %, again demonstrating the effectiveness and superiority of the proposed in-situ LADT process.

To further analyze the material removal mechanism of the high-entropy alloy CoCrFeMnNi and investigate the softening effects of the laser, a finite element model of the machining process was established. In this model, the sample was simplified as a rectangular block, with the bottom side fixed as the boundary conditions. The cutting tool was treated as a rigid body. Fig. 6 illustrates the simulation results of von-Mises equivalent stresses obtained by the commercial software ABAQUS. In the simulation of the SPDT process, the temperature of the workpiece was set to the room temperature of 20 °C, as shown in Fig. 6 (a). In order to investigate the softening effects of the laser heating, the

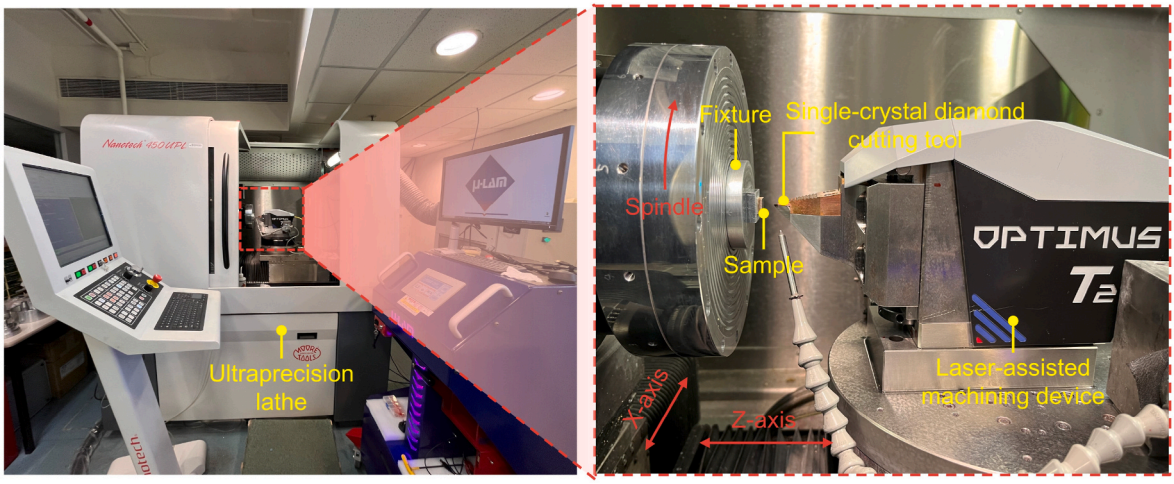

Fig. 3. Experimental setup of an in-situ LADT process.

Table 1
Cutting tool specification and detailed machining parameters.

Cutting tool specification		Detailed machining parameters			
Radius (mm)	1	Roughing machining		Finishing machining	
Flank angle	15°	Depth-of-cutting (μm)	5	Depth-of-cutting (μm)	2
Rake angle	−35°	Feed rate (mm/min)	2	Feed rate (mm/min)	1
		Spindle speed (RPM)	2000	Spindle speed (RPM)	2000

temperatures of the workpiece were set to 300 °C and 600 °C, as shown in Fig. 6(b) and (c). It can be observed that, in comparison to the SPDT process, the in-situ LADT process exhibits a significant reduction in von-Mises equivalent stress, which contributes to an enhancement in surface quality [42]. This phenomenon further serves as evidence that laser heating plays a role in enhancing surface quality.

3.2. X-ray diffraction analysis

X-ray diffraction (XRD) analysis was performed on sample surfaces to explore the crystalline structure after machining processes (in-situ LADT process and traditional SPDT process), as depicted in Fig. 7. The results imply that neither the in-situ LADT process nor SPDT process causes any significant alterations to the crystal structure, with only the face-centered cubic (FCC) structure observed in the XRD patterns. However, when compared to the unmachined surface, both in-situ LADT machined surface and SPDT machined surface exhibit increased peak intensities in the (111) plane while decreasing peak intensities in the (200) plane, suggesting that the removal of surface layers during machining may induce crystal reorientations [43]. As indicated in Fig. 7 (b–d), all three peaks of machined surfaces display a shift towards lower 2θ angles relative to the unmachined surface, indicating the introduction of small tensile stresses rather than compressive stress in the machined surfaces. This can be attributed to the dominant thermal effect during the machining process, which plays a more significant role than mechanical effects in generating residual stresses [44]. The smaller peak shift observed in the in-situ LADT machined surface compared to the SPDT machined surfaces may be attributed to the laser power employed in this experiment, which might not have been sufficient to induce severe thermal expansion.

In order to further investigate the effects of machining processes on the sample material, the electron backscatter diffraction (EBSD) tests were also conducted on the cross-section of samples by the scanning electron microscope apparatus attached to an EBSD detector, as shown

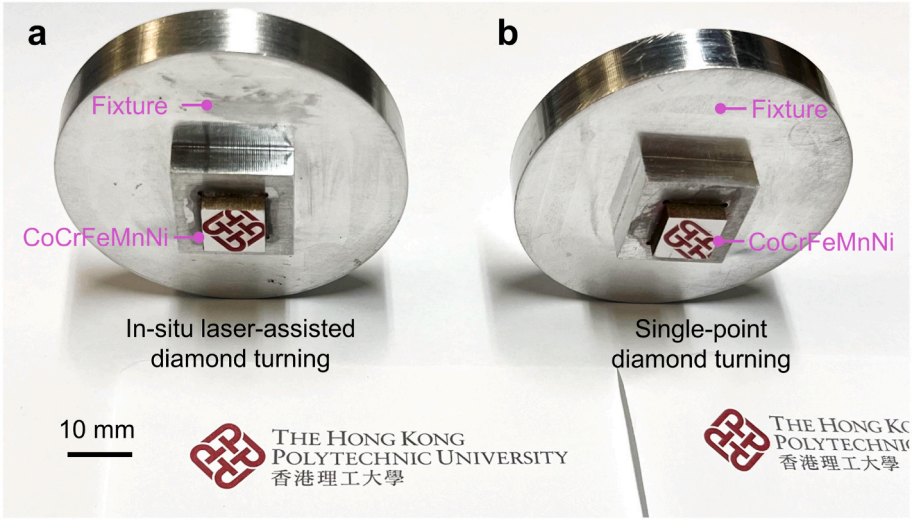

Fig. 4. Photographs of the mirror surfaces. (a) In-situ LADT machined surface and (b) SPDT machined surface.

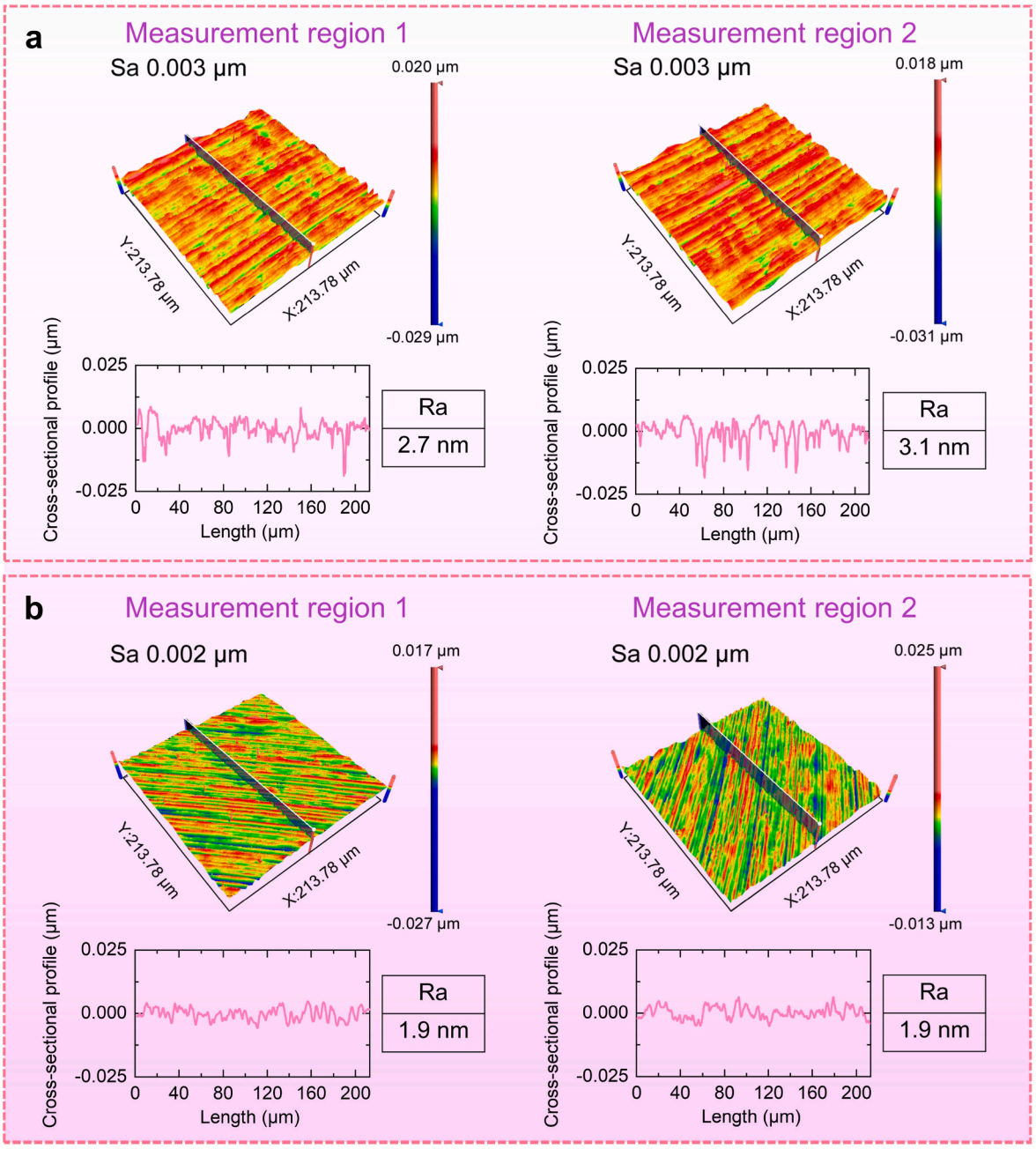

Fig. 5. Surface roughness and cross-sectional profile at two different measurement regions of machined sample surfaces. (a) SPDT process and (b) in-situ LADT process.

in Fig. 8. It can be found that the surfaces machined using the in-situ LADT process and the SPDT process show no significant differences, which is consistent with the XRD patterns because the absence of the broadening low peak after the in-situ LADT process and the SPDT process indicates that neither severe plastic deformation nor significant grain refinement was introduced [45].

Additionally, the kernel average misorientation (KAM) maps were also obtained to characterize the residual stress when conducting EBSD tests because the residual stress has direct influences on the sample mechanical properties and product life cycle [46,47]. Fig. 8 (c) and (d) depict the KAM maps along the cutting depth direction. It can be obviously found that the residual stress is mainly located on the top surface of samples. The affected layers are 83 μm and 138 μm thick for the in-situ LADT machined surface and SPDT machined surface, respectively. The proposed in-situ LADT process has a minor impact on the residual stress of samples when compared to the SPDT process, demonstrating its superiority.

3.3. Tool wear

Tool wear condition is also an important indicator to reflect the superiority of the proposed in-situ LADT process [48]. Fig. 9 shows the tool wear conditions of the traditional SPDT process and the proposed in-situ LADT process. It can be observed that both of them have tool wear, which is along the cutting edge. When machining the mirror surface, the cutting edge firstly contacts the sample surface, so it is easily worn. Besides, it is also found from the SEM images of the tool wear conditions that the flank wear is the main wear mechanism for the two different machining processes. There is adhesive wear for the traditional SPDT process, which occurs on the rake face.

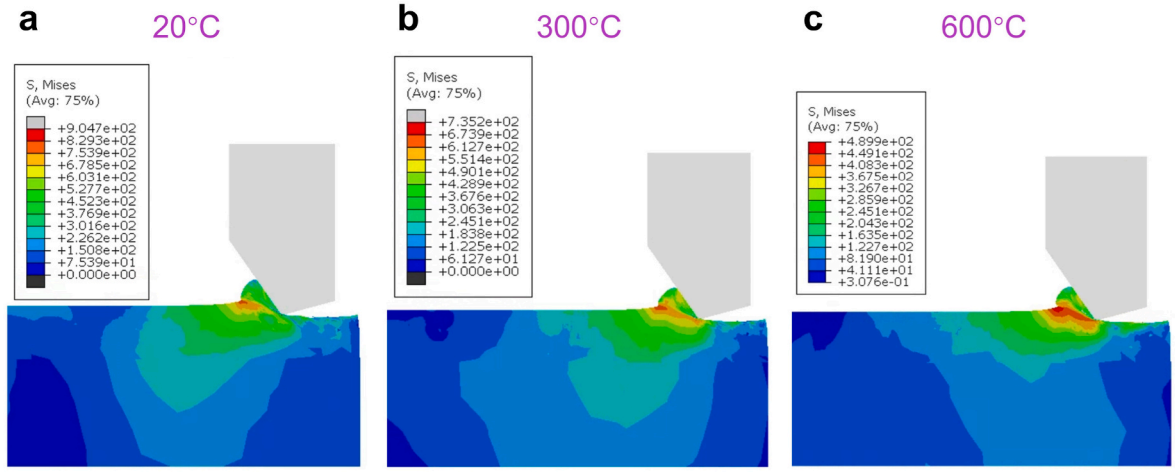

Fig. 6. Simulated von-Mises equivalent stress under different temperatures. (a) 20°, (b) 300°, and (c) 600°.

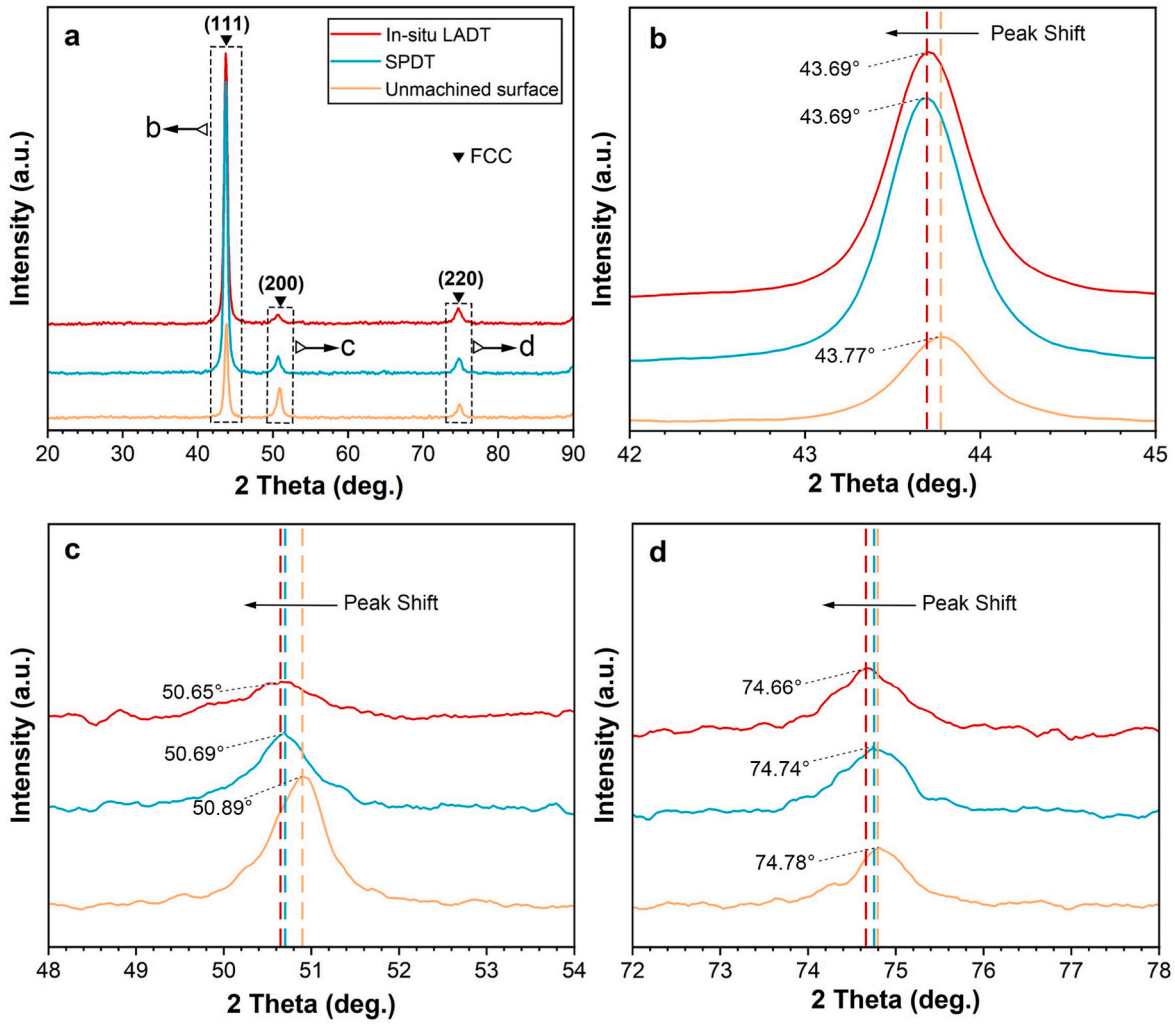

Fig. 7. XRD patterns of the workpiece surfaces generated by different processes. (a) Overview and (b–d) enlarged XRD peaks indicated in the areas of (a) for further analysis.

Table 2 shows the measurement results of the tool wear conditions. The wear length of the cutting tool for the traditional SPDT process is 255 μm while that for the proposed in-situ LADT process is only 161 μm, which is decreased by 36.9 %. Similarly, the wear width of the cutting tool is decreased by 49 % if using the proposed in-situ LADT process, which demonstrates the superiority of the proposed in-situ LADT process in decreasing the tool wear.

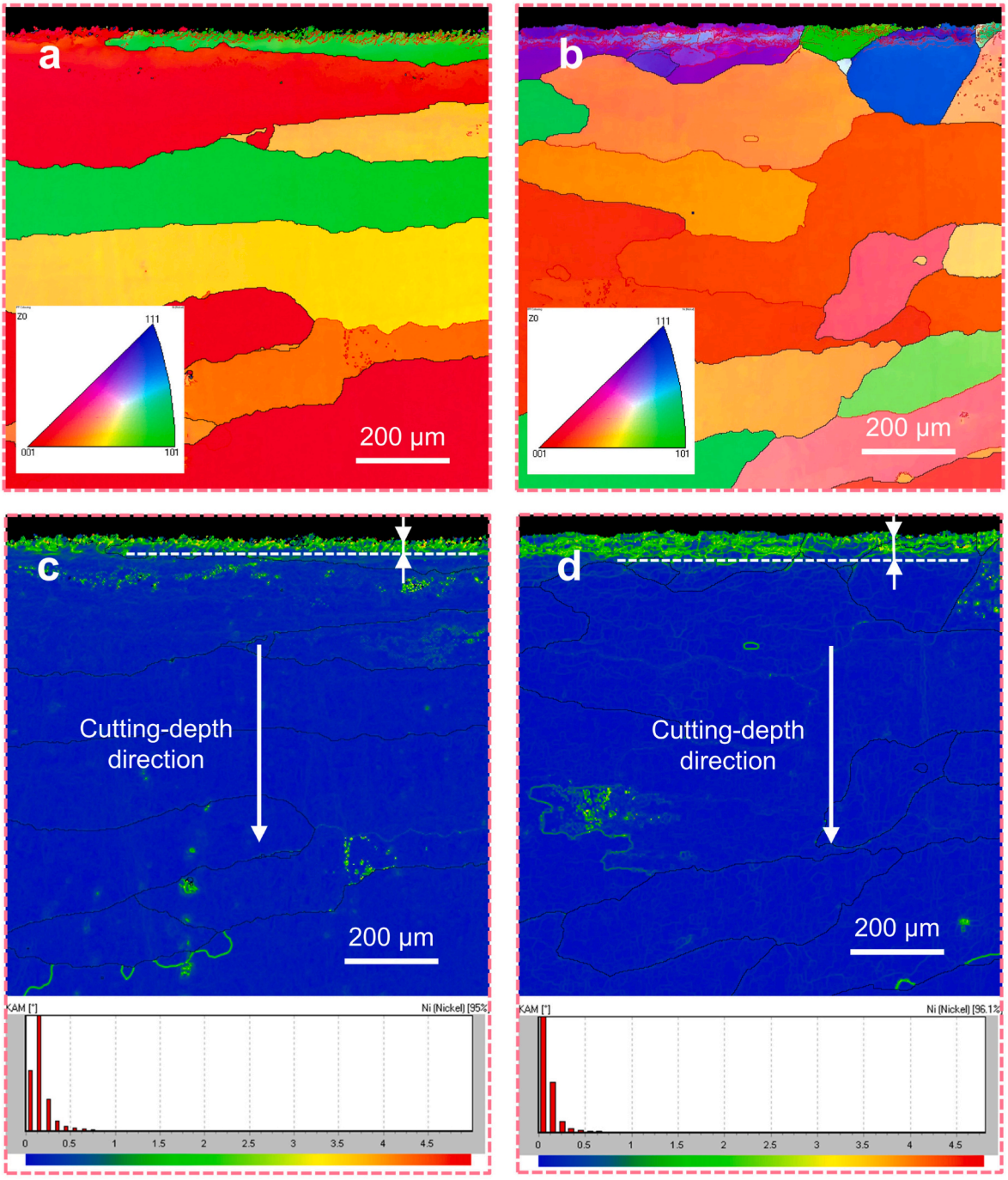

Fig. 8. EBSD images of (a) the in-situ LADT machined surface and (b) the SPDT machined surface. KAM maps of (c) the in-situ LADT machined surface and (d) the SPDT machined surface.

4. Conclusions

This study proposes an in-situ laser-assisted diamond turning (LADT) process to enhance the machinability of the high-entropy alloy CoCrFeMnNi. In this process, the in-situ laser-assisted machining is combined with the traditional single-point diamond turning process. A focused laser beam is used to soften the high-entropy alloy CoCrFeMnNi and a sharp diamond cutting tool is used to obtain the nanoscale surface quality.

Experimental results show the machined surface quality of the in-situ LADT process can reach 2 nm, which is improved by 33.3 %, demonstrating the effectiveness of the proposed machining process. The kernel average misorientation maps show the proposed in-situ LADT process has a minor impact on the crystal structure and the residual stress, showing the superiority of the proposed in-situ LADT process. Experimental results also find that the wear length of the single-crystal diamond cutting tool can decrease from 255 μm to 161 μm, further verifying the effectiveness of the proposed machining process in improving the machinability of the high-entropy alloy CoCrFeMnNi.

Therefore, this study not only provides an efficient machining method for enhancing the machinability of the high-entropy alloy but also helps engineers and researchers understand the material removal mechanism of the CoCrFeMnNi.

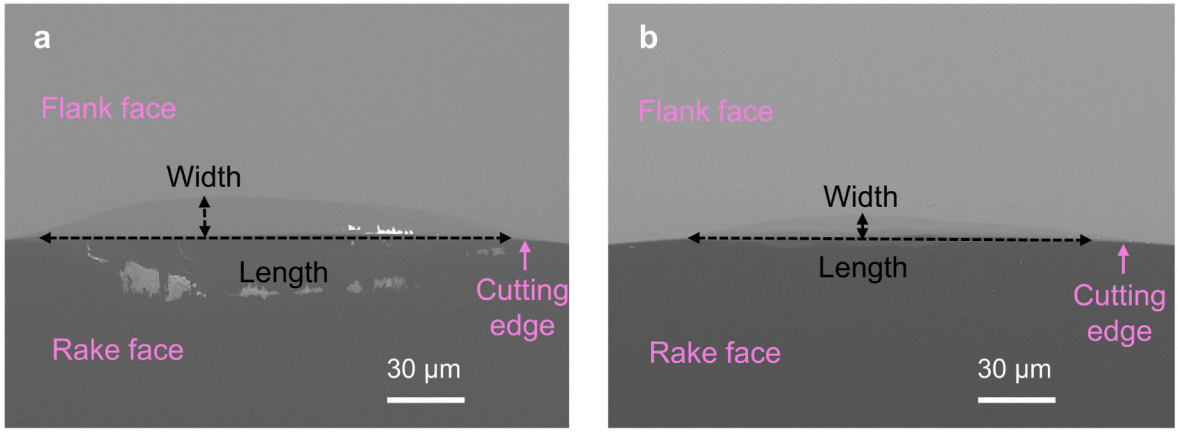

Fig. 9. SEM images of the tool wear. (a) The SPDT process and (b) the in-situ LADT process.

Table 2
Tool wear of different machining processes.

	Length (μm)	Width (μm)
Traditional SPDT process	255	20
In-situ LADT process	161	10.2
Percentage decrease	36.9 %	49 %

Data availability

The data will be made available upon reasonable request.

CRediT authorship contribution statement

Hanheng Du: Conceptualization, Methodology, Software, Validation, Formal analysis, Investigation, Data curation, Visualization, Writing – original draft, Writing – review & editing.**Yidan Wang:** Methodology, Writing – review & editing.**Yuhan Li:** Investigation.**Sen Yin:** Writing – review & editing.**Denghui Li:** Writing – review & editing. **Wai Sze Yip:** Writing – original draft, Writing – review & editing.**Suet To:** Supervision, Project administration, Funding acquisition, Resources, Writing – review & editing.

Declaration of competing interest

The authors declare that they have no known competing financial interests or personal relationships that could have appeared to influence the work reported in this paper.

Acknowledgements

This work was funded by the Research Grants Council of the Hong Kong Special Administrative Region, China (Project No.: PolyU 15221322), the National Natural Science Foundation of China (Project No.: U19A20104), the Shenzhen Science and Technology Program (Project No.: JCYJ20210324131214039), and State Key Laboratory of Ultra-precision Machining Technology.

References

[1] Miracle DB, Senkov ON. A critical review of high entropy alloys and related concepts. Acta Mater 2017;122:448–511.
[2] George EP, Raabe D, Ritchie RO. High-entropy alloys. Nat Rev Mater 2019;4:515–34. https://doi.org/10.1038/s41578-019-0121-4.
[3] Ruestes CJ, Farkas D. Dislocation emission and propagation under a nano-indenter in a model high entropy alloy. Comput Mater Sci 2022;205:111218. https://doi.org/10.1016/j.commatsci.2022.111218.
[4] Alabd Alhafez I, Ruestes CJ, Bringa EM, Urbassek HM. Nanoindentation into a high-entropy alloy – an atomistic study. J Alloys Compd 2019;803:618–24. https://doi.org/10.1016/j.jallcom.2019.06.277.
[5] He JY, Wang H, Huang HL, Xu XD, Chen MW, Wu Y, et al. A precipitation-hardened high-entropy alloy with outstanding tensile properties. Acta Mater 2016;102:187–96. https://doi.org/10.1016/j.actamat.2015.08.076.
[6] Tang Y, Wang R, Xiao B, Zhang Z, Li S, Qiao J, et al. A review on the dynamic-mechanical behaviors of high-entropy alloys. Prog Mater Sci 2023;135:101090. https://doi.org/10.1016/j.pmatsci.2023.101090.
[7] Xiong W, Guo AXY, Zhan S, Liu C-T, Cao SC. Refractory high-entropy alloys: a focused review of preparation methods and properties. J Mater Sci Technol 2023;142:196–215. https://doi.org/10.1016/j.jmst.2022.08.046.
[8] Lai K-C, Chao S-C, Tseng K-K, Yeh J-W, Chen P-Y. Biocompatible as-cast and homogenized TiNbTaZrMoV high entropy alloys: mechanical properties, corrosion resistance and in vitro studies. J Mater Res Technol 2023;24:9708–21. https://doi.org/10.1016/j.jmrt.2023.05.201.
[9] Garcia Filho FDC, Ritchie RO, Meyers MA, Monteiro SN. Cantor-derived medium-entropy alloys: bridging the gap between traditional metallic and high-entropy alloys. J Mater Res Technol 2022;17:1868–95. https://doi.org/10.1016/j.jmrt.2022.01.118.
[10] Batchelor TAA, Pedersen JK, Winther SH, Castelli IE, Jacobsen KW, Rossmeisl J. High-entropy alloys as a discovery platform for electrocatalysis. Joule 2019;3:834–45. https://doi.org/10.1016/j.joule.2018.12.015.
[11] Kumar D. Recent advances in tribology of high entropy alloys: a critical review. Prog Mater Sci 2023;136:101106. https://doi.org/10.1016/j.pmatsci.2023.101106.
[12] Guo Y, Su H, Yang P, Zhao Y, Shen Z, Liu Y, et al. A review of emerging metallic system for high-energy beam additive manufacturing: Al–Co–Cr–Fe–Ni high entropy alloys. Acta Metall Sin (English Lett 2022;35:1407–23. https://doi.org/10.1007/s40195-022-01400-y.
[13] Kim Y-K, Kim M-C, Lee K-A. 1.45 GPa ultrastrong cryogenic strength with superior impact toughness in the in-situ nano oxide reinforced CrMnFeCoNi high-entropy alloy matrix nanocomposite manufactured by laser powder bed fusion. J Mater Sci Technol 2022;97:10–9. https://doi.org/10.1016/j.jmst.2021.04.030.
[14] Li H, Lai J, Li Z, Wang L. Multi-sites electrocatalysis in high-entropy alloys. Adv Funct Mater 2021;31:2106715. https://doi.org/10.1002/adfm.202106715.
[15] Tsai M-H, Yeh J-W. High-entropy alloys: a critical review. Mater Res Lett 2014;2:107–23. https://doi.org/10.1080/21663831.2014.912690.
[16] Zhao S, Li Z, Zhu C, Yang W, Zhang Z, Armstrong DEJ, et al. Amorphization in extreme deformation of the CrMnFeCoNi high-entropy alloy. Sci Adv 2023;7:eabb3108. https://doi.org/10.1126/sciadv.abb3108.
[17] Kaushik N, Meena A, Mali HS. High entropy alloy synthesis, characterisation, manufacturing & potential applications: a review. Mater Manuf Process 2022;37:1085–109. https://doi.org/10.1080/10426914.2021.2006223.
[18] Garcia Filho FC, Monteiro SN. Welding joints in high entropy alloys: a short-review on recent trends. Materials 2020;13:1411. https://doi.org/10.3390/ma13061411.
[19] Alshataif YA, Sivasankaran S, Al-Mufadi FA, Alaboodi AS, Ammar HR. Manufacturing methods, microstructural and mechanical properties evolutions of high-entropy alloys: a review. Met Mater Int 2020;26:1099–133. https://doi.org/10.1007/s12540-019-00565-z.
[20] Kim J, Wakai A, Moridi A. Materials and manufacturing renaissance: additive manufacturing of high-entropy alloys. J Mater Res 2020;35:1963–83. https://doi.org/10.1557/jmr.2020.140.
[21] Cagirici M, Wang P, Ng FL, Nai MLS, Ding J, Wei J. Additive manufacturing of high-entropy alloys by thermophysical calculations and in situ alloying. J Mater Sci Technol 2021;94:53–66. https://doi.org/10.1016/j.jmst.2021.03.038.
[22] Ostovari Moghaddam A, Shaburova NA, Samodurova MN, Abdollahzadeh A, Trofimov EA. Additive manufacturing of high entropy alloys: a practical review. J Mater Sci Technol 2021;77:131–62. https://doi.org/10.1016/j.jmst.2020.11.029.
[23] Han C, Fang Q, Shi Y, Tor SB, Chua CK, Zhou K. Recent advances on high-entropy alloys for 3D printing. Adv Mater 2020;32:1903855.

[24] John M, Diaz O, Esparza A, Fliegler A, Ocenosak D, Van Dorn C, et al. Welding techniques for high entropy alloys: processes, properties, characterization, and challenges. Materials 2022;15. https://doi.org/10.3390/ma15062273.
[25] Li J, Chen H, Fang Q, Jiang C, Liu Y, Liaw PK. Unraveling the dislocation–precipitate interactions in high-entropy alloys. Int J Plast 2020;133:102819.
[26] Guo J, Goh M, Zhu Z, Lee X, Nai MLS, Wei J. On the machining of selective laser melting CoCrFeMnNi high-entropy alloy. Mater Des 2018;153:211–20. https://doi.org/10.1016/j.matdes.2018.05.012.
[27] Mohammadi H, Ravindra D, Kode SK, Patten JA. Experimental work on micro laser-assisted diamond turning of silicon (111). J Manuf Process 2015;19:125–8. https://doi.org/10.1016/j.jmapro.2015.06.007.
[28] Du H, Yip WS, Sun W, Kang C, To S. In-situ laser-assisted ultraprecision cutting of WC-Co cemented carbide for creating microstructure arrays. Ceram Int 2023;49:38698–707. https://doi.org/10.1016/j.ceramint.2023.09.206.
[29] You K, Fang F, Yan G. Surface generation of tungsten carbide in laser-assisted diamond turning. Int J Mach Tool Manufact 2021;168:103770. https://doi.org/10.1016/j.ijmachtools.2021.103770.
[30] Du H, Chen H, Zhu Z, Wang Z, To Suet. Novel hybrid machining process of titanium alloy for texturing high-quality microstructure array surfaces. Surf Coating Technol 2023;462:129494. https://doi.org/10.1016/j.surfcoat.2023.129494.
[31] Wang M, Zheng Z, Wu Z, Zhang J, Chen X, Xiao J, et al. Investigation on the machinability of SiCp/Al composite by in-situ laser assisted diamond cutting. J Mater Process Technol 2023;318:118044. https://doi.org/10.1016/j.jmatprotec.2023.118044.
[32] Lin C, Chen X, He W, Xu G, Liu C, Zhang J, et al. Experimental investigation on the ductile machinability of fused silica during in-situ laser assisted diamond cutting. J Manuf Process 2022;84:383–93. https://doi.org/10.1016/j.jmapro.2022.10.005.
[33] Huang K, Shen Z, Zheng Z, Lin C, Huang W, Zhang J, et al. Investigation on the machinability of nitriding mold steel by applying in-situ laser assisted diamond cutting. J Manuf Process 2022;84:149–61. https://doi.org/10.1016/j.jmapro.2022.09.055.
[34] You K, Yan G, Luo X, Gilchrist MD, Fang F. Advances in laser assisted machining of hard and brittle materials. J Manuf Process 2020;58:677–92. https://doi.org/10.1016/j.jmapro.2020.08.034.
[35] You K, Fang F. High effective laser assisted diamond turning of binderless tungsten carbide. J Mater Process Technol 2022;302:117505. https://doi.org/10.1016/j.jmatprotec.2022.117505.
[36] Zhang H, Zeng H, Yan R, Wang W, Peng F. Analytical modeling of cutting forces considering material softening effect in laser-assisted milling of AerMet100 steel. Int J Adv Manuf Technol 2021;113:247–60. https://doi.org/10.1007/s00170-020-06518-w.
[37] Zhang J, Fu Y, Chen X, Shen Z, Zhang J, Xiao J, et al. Investigation of the material removal process in in-situ laser-assisted diamond cutting of reaction-bonded silicon carbide. J Eur Ceram Soc 2023;43:2354–65. https://doi.org/10.1016/j.jeurceramsoc.2023.01.011.
[38] Wei Y, Li S, Shi F, Wang X, Park SS. Improved direct laser assisted machining of Al 7075-T6 and Ti-6Al-4V using cubic zirconia tool. J Manuf Process 2023;101:501–11. https://doi.org/10.1016/j.jmapro.2023.06.026.
[39] Li C, Hu Y, Zhang F, Geng Y, Meng B. Molecular dynamics simulation of laser assisted grinding of GaN crystals. Int J Mech Sci 2023;239:107856. https://doi.org/10.1016/j.ijmecsci.2022.107856.
[40] Hao Z, Gao D, Fan Y, Han R. New observations on tool wear mechanism in dry machining Inconel718. Int J Mach Tool Manufact 2011;51:973–9. https://doi.org/10.1016/j.ijmachtools.2011.08.018.
[41] Malakizadi A, Hajali T, Schulz F, Cedergren S, Ålgårdh J, M'Saoubi R, et al. The role of microstructural characteristics of additively manufactured Alloy 718 on tool wear in machining. Int J Mach Tool Manufact 2021;171:103814. https://doi.org/10.1016/j.ijmachtools.2021.103814.
[42] Ding H, Shen N, Shin YC. Thermal and mechanical modeling analysis of laser-assisted micro-milling of difficult-to-machine alloys. J Mater Process Technol 2012;212:601–13. https://doi.org/10.1016/j.jmatprotec.2011.07.016.
[43] Zhang L, Hashimoto T, Yan J. Machinability exploration for high-entropy alloy FeCrCoMnNi by ultrasonic vibration-assisted diamond turning. CIRP Ann 2021;70:37–40. https://doi.org/10.1016/j.cirp.2021.04.090.
[44] Pramanik A, Zhang LC, Arsecularatne JA. Machining of metal matrix composites: effect of ceramic particles on residual stress, surface roughness and chip formation. Int J Mach Tool Manufact 2008;48:1613–25. https://doi.org/10.1016/j.ijmachtools.2008.07.008.
[45] Xu D, Liao Z, Axinte D, Sarasua JA, M'Saoubi R, Wretland A. Investigation of surface integrity in laser-assisted machining of nickel based superalloy. Mater Des 2020;194:108851. https://doi.org/10.1016/j.matdes.2020.108851.
[46] Denkena B, Boehnke D, de León L. Machining induced residual stress in structural aluminum parts. Prod Eng 2008;2:247–53. https://doi.org/10.1007/s11740-008-0097-1.
[47] Singh A, Agrawal A. Investigation of surface residual stress distribution in deformation machining process for aluminum alloy. J Mater Process Technol 2015;225:195–202. https://doi.org/10.1016/j.jmatprotec.2015.05.025.
[48] Du H, Jiang M, Wang Z, Zhu Z, To S. Generating micro/nanostructures on magnesium alloy surface using ultraprecision diamond surface texturing process. J Magnesium Alloys 2023;11:1472–83. https://doi.org/10.1016/j.jma.2022.07.018.